Structure, stability and defect energetics of interfaces formed between conventional and transformed phases in Cu-Nb layered nanocomposite

Saikia, Ujjal; Sahariah, Munima B.; Dutta, Biswanath; Pandey, Ravindra

DOI
10.1088/1402-4896/acd5b3

Publication date
2023

Document Version
Final published version

Published in
Physica Scripta

PAPER

Structure, stability and defect energetics of interfaces formed between conventional and transformed phases in Cu–Nb layered nanocomposite

Physica Scripta

PAPER

Structure, stability and defect energetics of interfaces formed between conventional and transformed phases in Cu–Nb layered nanocomposite

RECEIVED
10 February 2023

REVISED
3 May 2023

ACCEPTED FOR PUBLICATION
15 May 2023

PUBLISHED
30 May 2023

Ujjal Saikia[1,2], **Munima B Sahariah**[1,*], **Biswanath Dutta**[3] **and Ravindra Pandey**[4]

[1] Institute of Advanced Study in Science and Technology, Guwahati 781035, India
[2] Max-Planck-Institut für Eisenforschung GmbH, Max-Planck-Str. 1, D-40237 Düsseldorf, Germany
[3] Materials Science and Engineering, Delft University of Technology, 2628 CD, Delft, The Netherlands
[4] Department of Physics, Michigan Technological University, Houghton, MI 49931-1295, United States of America
[*] Author to whom any correspondence should be addressed.

E-mail: ujjalsaikia79@gmail.com **and** munima@iasst.gov.in

Keywords: Cu–Nb layered nanocomposite, interface structure and stability, uniaxial tensile simulation, defect energetics

Supplementary material for this article is available online

Abstract

Layered nanocomposite material having fcc-bcc interface with Kurdjumov-Sachs interface orientation relation has shown great potential as radiation resistant structural material for future fusion energy reactors. The superior radiation resistant properties of this material are attributed to it's special fcc-bcc interface structure. In this study we have reported a stable interface between conventional bcc phase of Nb and transformed bcc phase of Cu. This bcc-bcc interface is found to be stable from both strain-energy and dynamical stability analysis. We have also shown that the bcc-bcc interface has different defect energetics behaviour compared to previously reported fcc-bcc interface which has a negative impact on the self annihilation property of the material against radiation induced defects. These aspects should be carefully considered in the future design of robust layered material for extreme radiation environment.

1. Introduction

Development of high-performance structural materials is a critical aspect for the future success of proposed fusion energy reactors [1–3]. These structural materials have to withstand unprecedented fluxes of high-energy neutrons along with intense thermomechanical stresses. Extensive research has already been devoted toward this direction with focus on either enhancement of the existing materials or developing new novel materials, for example, ferritic/martensitic steel with W and V, oxide dispersion strengthened steel, refractory alloys based on either V or W, SiC/SiC ceramic composites [2, 4–6]. Layered nanocomposites with interface between two dissimilar metals have shown great promise for such applications which can be attributed to their large volume fraction of interfaces and unique interface morphology. These interfaces may act as a barrier to slip and sinks for radiation induced damages [7, 8]. However, properties like defect sink strength [9, 10], susceptibility to embrittlement [11], mechanical strength [12, 13], diffusivity [14] of the materials may differ with atomic structure of the interfaces. Also, in some cases, interfaces may limit the overall lifetime of a material by increasing the free energy of the system [15]. Therefore, only having large fraction of interfaces is not sufficient for a material to perform reliably under irradiation. They must also have the right thermodynamic, kinetic and mechanical properties.

The fcc-bcc metallic interfaces between two immiscible metals such as Cu–Nb, Cu-V, Cu-W, Al-Fe, Al-Nb and Cu-Mg draw significant research attention [16–21]. Among them, one of the widely explored promising material for such application is Cu–Nb layered nanocomposite system. Extensive research on Cu–Nb confirms elevated morphological stability of the interface under thermomechanical stresses [18, 22–24], self annihilation of radiation induced point defects [25, 26] and retardation of He bubble growth [27, 28]. Atomistic simulations

suggests the possibility of making tailored Cu–Nb interfaces that are virtually inexhaustible sinks for radiation-induced point defects and catalysts for efficient Frenkel pair recombination [25]. Therefore, Cu–Nb can be considered as a promising test bed for investigating the role of fcc-bcc interfaces in the quest of fusion structural material research.

The key feature responsible for such excellent mechanical property and radiation resistance behavior of this Cu–Nb layered nanocomposite system is it's fcc-bcc interface structure with Kurdjumov-Sachs (KS) interface orientation relation [29]. However, there are experimental evidence which reported growth of slightly distorted bcc phase of Cu instead of fcc phase at layer thickness below 12 Å [30, 31]. Above this layer thickness the bcc Cu loses coherency and transforms martensitically to the fcc phase. Based on molecular dynamics (MD) simulations study of the deposition process J Wang *et al* [32] showed that for smaller layer thickness deposited Cu layer initially grows as bcc on the bcc Nb substrate. Therefore, one can expect that during deposition of Cu on a bcc Nb substrate, Cu will start to grow as bcc from the beginning up to layer thickness of ~12 Å. Conversely, J Y Zhang *et al* [33] reported phase transition of Nb from bcc to fcc in Cu–Nb. Growth of such metastable phases of a material on the substrate of another material with different phase is interesting but not unusual. For example, growth of fcc films of Nb on quartz substrate [34], bcc Cu films deposited on Ag (100), Fe (001) and Au (100) [35–37] substrates has already been confirmed experimentally.

Such growth will change the unique fcc-bcc interface structure with KS orientation which was identified as the key feature of the Cu–Nb system. This will definitely impact mechanical property and radiation resistance behavior of the conventional Cu–Nb interface. Despite of such importance, knowledge on bcc-bcc or fcc-fcc interface between Cu and Nb is still limited. Strain induced bcc to fcc phase transformation for molybdenum at crack tips during straining was already reported by S J Wang *et al* [38]. As evidenced by scanning transmission electron microscopy and nanodiffraction, the observed fcc phase appears to be a well-defined metastable state. Considering these facts and possibility of phase transformation from bcc to fcc or vice-versa in Cu–Nb under extreme thermomechanical stresses, we believe that knowledge about the stability and interface behaviour of Cu–Nb nanocomposite with transformed phases is extremely important.

In this study we have addressed the mechanical stability of the bcc-bcc and fcc-fcc Cu–Nb layered system using density functional theory (DFT) [39] based strain-energy calculation and dynamical stability using density functional perturbation theory (DFPT) [40, 41]. For a systematic comparison, we have started with both stable and unstable bulk phases of Cu and Nb, followed by free-standing slabs and layered nanocomposites with interface between stable and unstable phases (Cu_{bcc}-Nb_{bcc} and Cu_{fcc}-Nb_{fcc}). Only Cu_{bcc}-Nb_{bcc} interface was found stable. Further, we performed uniaxial tensile test (UTS) to understand decohesion behavior of this new interface. Nature of interaction between Cu and Nb atoms at the interface and defect energetics at the interface was also investigated in this study by electronic density of states (DOS), charge density difference and vacancy formation energy analysis.

2. Computational details

The projector-augmented wave (PAW) [42] method as implemented in the Vienna *Ab-initio* Simulation Package (VASP) [43] was used for all the DFT [39] and DFPT [40, 41] calculations. Corrections to the non-local exchange and correlation energies were treated using the generalized-gradient approximation (GGA) [44]. Norm-conserving pseudo potentials with seventeen valence electrons for Cu ($3p^6 3d^{10} 4s^1$) and eleven for Nb ($4p^6 4d^4 5s^1$) were used in the calculations. Plane waves with a kinetic energy cutoff of 500eV were used to expand the Kohn–Sham orbitals. We used 1E-08 eV energy convergence parameter for electronic self-consistent part with 0.001 eV $Å^{-1}$ maximum forces on every relaxed atom. The brillouin zone (BZ) summations were carried out with Monkhorst–Pack grid [45]. Further computational details are provided in the supplemental material available with this article.

3. Results

3.1. Structure and stability analysis

For calculation of the cubic fcc and bcc bulk phases, we used rhombohedral primitive unitcells. The procedure as described in reference [46] was followed during calculation of the three independent elastic stiffness constants (C_{11}, C_{12} and C_{44}) of the cubic phases. We obtained quite small energy difference (40 meV $Atom^{-1}$) between Cu_{fcc} and Cu_{bcc}. Previous studies also suggest that depending on the approximations used (augmented spherical wave, pseudopotential, all electron method, etc.) energy difference may vary from 7–48 meV $Atom^{-1}$ [26, 47]. The Cu_{bcc} phase is not stable under the volume-conserving orthorhombic strain, which leads to the violation of one of the Born mechanical stability criteria for cubic crystal [48], C_{11}–$C_{12} > 0$, with a negative value for the shear modulus (−8.96 GPa). As shown in figure 1 (a), this instability results in imaginary phonon branch

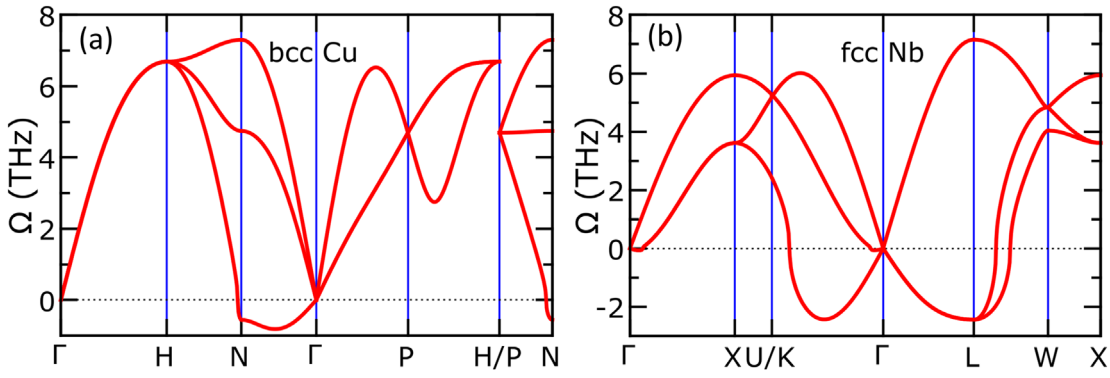

Figure 1. Calculated phonon dispersion curves for bcc Cu and fcc Nb plotted along high-symmetry directions in the Brillouin zone. As evidenced by the negative phonon frequencies these transformed bulk phases are not stable.

Table 1. The optimized in-plane lattice parameters (a_x and a_y in Å), interlayer separation (d in Å) and planner elastic stiffness constants (C_{11}, C_{12} and C_{22} in GPa) for the free-standing slabs.

System	a_x	a_y	d	C_{11}	C_{12}	C_{22}
fcc Cu	2.54	4.41	2.10	291.78	149.93	266.78
bcc Cu	2.66	4.22	2.11	251.29	148.44	323.35
bcc Nb	3.29	4.48	2.38	301.43	196.92	342.77
fcc Nb	2.94	5.10	2.42	260.18	235.11	220.97

(depicted as negative value of frequency) in the first brillouin zone (BZ). Similarly, fcc phase of Nb has slightly higher energy (0.33 eV atom^{-1}) than it's conventional stable bcc phase. The Nb_{fcc} phase is not stable under tri-axial shear strain and volume-conserving orthorhombic strain, which leads to the violation of two of the Born mechanical stability criteria for cubic crystal [48], C_{11}–$C_{12} > 0$ and $C_{44} > 0$, with negative value of shear modulus (−122.20 GPa) and negative value of C_{44} (−50.23 GPa). The instability of Nb_{fcc} can also be realized from the presence of imaginary phonon modes in figure 1(b). These results confirms that at ideal condition, bcc phase of Cu and fcc phase of Nb are not stable.

We performed similar calculations on the free-standing slabs of both Cu and Nb. We have considered (110) slabs of Cu_{bcc} and (111) slabs of Nb_{fcc}. For a systematic comparison, Cu_{fcc} (111) and Nb_{bcc} (110) slabs were also considered in this study. The fcc (111) and bcc (110) slab were modeled using nonprimitive orthorhombic unit cells (Further technical details for construction of the slabs are provided in the supplemental material). The optimized in-plane lattice parameters and interplanar separation for the free-standing slabs are tabulated in table 1. Comparing them with the fcc (111) and bcc (110) planes of the corresponding bulk counterparts we observed minimal rearrangement of the in-plane lattice parameter a_x (1.17%, 8.29%, 0.91%, 1.69%), a_y (0.90%, −3.37%, 4.79%, 1.56%), and interlayer separation d (−0.48%, −3.37%, −1.27%, 0.82%) for the Cu_{fcc}(111), Cu_{bcc}(110), Nb_{bcc}(110) and Nb_{fcc}(111) slabs respectively. The positive and negative values indicate compression and expansion compared to the respective bulk phases.

The elastic stiffness coefficients C_{11}, C_{22}, and C_{12} of the slabs were obtained by fitting the DFT-calculated unit-cell energy to a series of 2-dimensonal strain states (ϵ_{ij}) as described in reference [49]. As expected, the (111) slab of Cu_{fcc} and (110) slab of Nb_{bcc} are mechanically stable under the applied uniaxial and biaxial strains, i.e., they satisfy the Born's criteria for mechanical stability [50], C_{11}-$C_{12} > 0$ (table 1). The in-plane Young's modulus along x direction of the slabs are 8.95% larger for Cu_{fcc} (111) and 12.83% smaller for Nb_{bcc} (110) than the y direction, suggesting that the in-plane Young's modulus of both the slabs are direction dependent and the slabs are more flexible in one direction than the other. This difference arises due to the anisotropic structure of the slabs and inherent difference in topology of the fcc (111) and bcc (110) lattice planes. The absence of any imaginary phonon frequency in the BZ as depicted in figures 2(a) and (c) also suggests the stability of these two free-standing slabs.

Contrary to expectation, the calculated stiffness constants suggest that the Cu_{bcc}(110) slab is mechanically stable (table 1). Compared to the Cu_{fcc}(111) slab, the in-plane Young's modulus of this slab is 12.48% smaller along x direction and 21.59% larger along y direction. However, as shown in figure 2(b), we have found imaginary phonon frequencies, suggesting dynamical instability of the slab. For Nb_{fcc}(111) slab, stiffness constants (table 1) and phonon dispersion (figure 2(d)) confirm it's mechanical and dynamical instability. Our

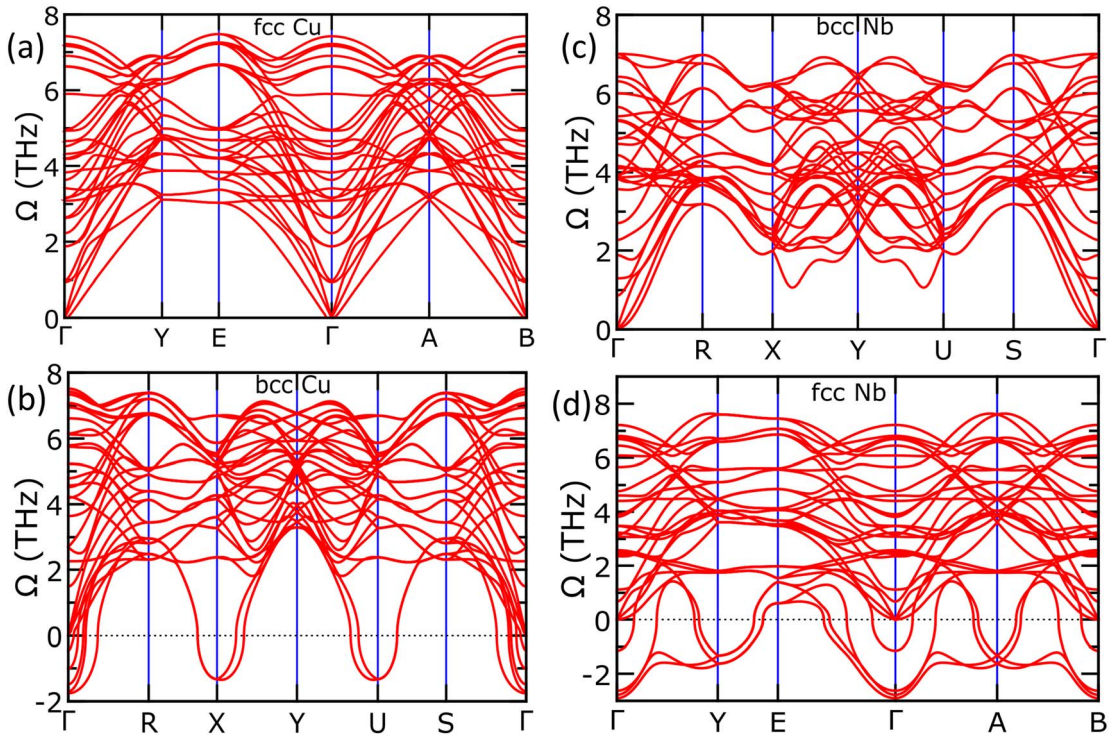

Figure 2. Calculated phonon dispersion curves of the free-standing slabs. (a) Cu_{fcc}(111), (b) Nb_{bcc}(110), (c) Cu_{bcc}(110), and (d) Nb_{fcc}(111). The considered free-standing slabs for the conventional phases (fcc for Cu and bcc for Nb) are stable as evidenced by absence of any negative phonon frequencies. The negative phonon frequencies appeared for the transformed free-standing slabs (bcc for Cu and fcc for Nb) implies that these structures are not stable.

findings for bulk and slab structures thus raise expectations that unusual structural and dynamical features may occur at the interface of the stable/unstable Cu–Nb layered nanocomposite system.

Having studied the stability of bulk and free-standing slab systems, we now investigate the consequences of growing bcc phase of Cu on bcc Nb and fcc phase of Nb on fcc Cu. To that end, we have constructed layered nanocomposite systems with Cu_{bcc}(110)–Nb_{bcc}(110) and Cu_{fcc}(111)–Nb_{fcc}(111) interfaces. Initial structures were modelled by joining the optimized bcc (fcc) slab of Cu to the bcc (fcc) slab of Nb in a orthorhombic simulation box. To overcome small differences in the in-plane lattice parameters, we applied a nominal strain to both Cu and Nb. Finally, full relaxation of the structures were performed. Based on different termination of the interfacial atomic plane of the Cu slab, two different initial interface structures for Cu_{bcc}(110)–Nb_{bcc}(110) (interface 1 and interface 2 as shown in figures 3(a) and (b), and two for Cu_{fcc}(111)–Nb_{fcc}(111) (interface 3 and interface 4 as shown in figures 3(c) and (d)) were considered in this study.

For bcc-bcc configuration, lattice parameters along x and y direction (a_x and a_y) of interface 1 system differs from any of the parent systems with difference of 7.38% and 8.05% from bcc Nb bulk and slab and 20.94% and 29.10% from bcc Cu bulk and slab respectively. For interface 2, negligible difference from the lattice parameters of bcc Nb bulk (0.93%) and bcc Nb slab (0.03%) was observed. Whereas, we observed a large difference with respect to bcc Cu bulk (12.98%) and slab (21.21%). This can be well understood from the value of bulk modulus. Nb has larger bulk modulus and hence stiffer than Cu (Supplemental material: table SM I). Therefore, Cu undergoes larger changes for both interface 1 and interface 2. The separation between first neighbouring interfacial Cu and Nb layers is 2.06 Å(2.65 Å) for the interface 1 (interface 2), which is 13.15% smaller (20.27% larger) than the separation we have reported for Cu_{fcc}(111)-Nb_{bcc}(110) semicoherent interface in our previous study [51]. The larger interfacial separation in case of interface 2 can be realized from the coherency induced repulsion between the immiscible Cu–Nb interface. The interface 2 minimizes it's energy by increasing the interfacial separation and the interface 1 does the same by relaxing the lattice parameters along x and y direction.

The interface 1 is energetically more favourable than interface 2 having energy difference of 0.14 eV $atom^{-1}$. However, calculation of elastic stiffness constants suggest that both the systems are mechanically stable (table 2) as per the six necessary and sufficient Born criteria for an orthorhombic crystal [48]. Following the definition of Pugh (G/B less than 0.5 for a ductile material), our calculations suggest both bcc-bcc systems represent ductile behaviour [52]. This is further supported by the value of Poission's ratio of 0.41 (less than 0.33 for brittle materials). The phonon dispersion curve of the interface 2 as shown in figure 4 (a) suggest that the system is dynamically not stable. Only the interface 1 shows dynamical stability as depicted in figure 4(b).

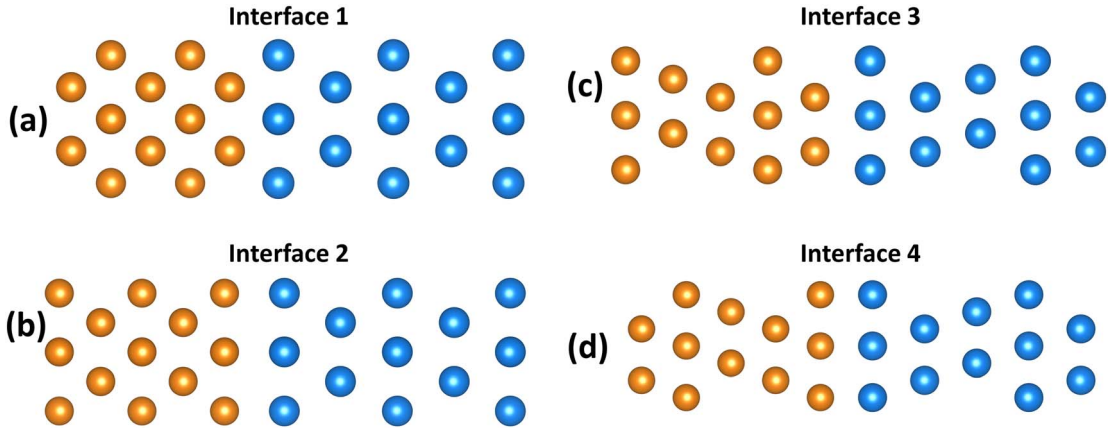

Figure 3. The configuration of the different Cu–Nb interfaces considered in this study. Top views of the Cu_{bcc}(110)–Nb_{bcc}(110) (a) interface 1, and (b) interface 2; top view of the Cu_{fcc}(111)-Nb_{fcc}(111) (c) interface 3, and (d) interface 4.

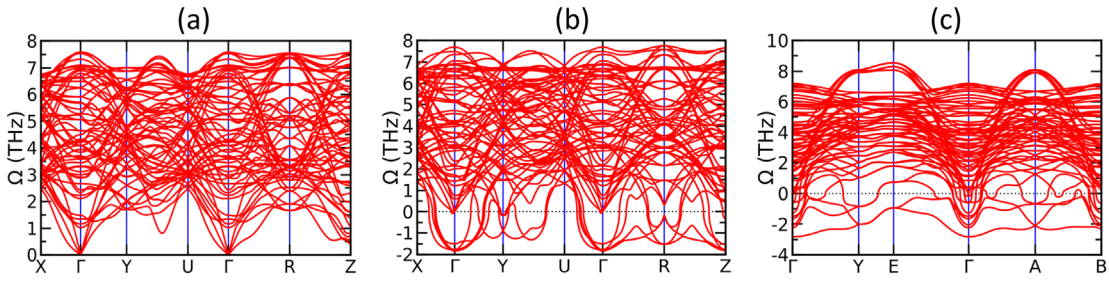

Figure 4. Calculated phonon dispersion curves for the layered nanocomposite systems. Cu_{bcc}(110)-Nb_{bcc}(110): (a) interface 1 and (b) interface 2, and (c) Cu_{fcc}(111)–Nb_{fcc}(111) interface.

Table 2. Calculated elastic stiffness constants (in GPa) for interface 1 and interface 2 of Cu_{bcc}–Nb_{bcc} and Cu_{fcc}–Nb_{fcc} interface.

	C_{11}	C_{22}	C_{33}	C_{44}	C_{55}	C_{66}	C_{12}	C_{13}	C_{23}	C_{15}	C_{25}	C_{35}	C_{46}
interface 1:	219.4	193.4	152.6	19.5	49.0	48.4	152.6	117.5	143.3	—	—	—	—
interface 2:	238.4	197.1	130.7	10.4	24.3	60.0	130.7	106.2	144.8	—	—	—	—
Cu_{fcc}–Nb_{fcc}:	125.3	89.7	109.0	31.2	2.0	−1.8	57.6	56.3	65.9	100.2	100.3	100.7	0.4

In case of Cu_{fcc}(111)-Nb_{fcc}(111), structural optimization of both the interface 3 and interface 4 orthorhombic structures converged to a similar monoclinic structure. The lattice parameters along x and y direction (a_x and a_y) of this monoclinic system is noticeably different from the corresponding lattice parameters of fcc Cu bulk (3.73%) and fcc Cu slab (4.86%), which is even larger in comparison to fcc Nb bulk (11.54%) and fcc Nb slab (9.76%). With a negative value of C_{66} (table 2), this fcc-fcc system shows mechanical instability. The presence of imaginary phonon modes further suggest dynamical instability of the system (figure 4(c)).

3.2. Decohesion behavior and defect energetics

Among all four considered interfacial configurations, only interface 1 between bcc Cu and bcc Nb was found stable from both strain-energy and phonon dispersion analysis. Therefore, at the first step we performed uniaxial tensile simulation (UTS) to study decohesion behavior of this interface. We applied a series of uniaxial tensile strain perpendicular to the interface and calculated the corresponding stress from the total energy of the strained systems. For each initial strained configurations, ions were allowed to relax until forces on each ions converges below 0.001 eV $Å^{-1}$. As evidenced by the stress-strain curve in figure 5, strength of Cu–Nb bcc-bcc interface is less than their bulk counterpart (i.e, Cu in fcc bulk and Nb in bcc bulk crystal structure). We observed fracture at the interface with strain value below 0.2. As we have shown in this work and also reported in previous studies [47, 53], bulk bcc phase of Cu has a weak shear modulus $G = (C_{11} - C_{12})/2$. Hence, this phase will offer no resistance to (110) shears. In case of Cu–Nb system, the bcc phase of Cu on top of bcc Nb substrate become stable only because of the coherency strain induced by the substrate. Therefore, the bcc-bcc Cu–Nb interface is vulnerable

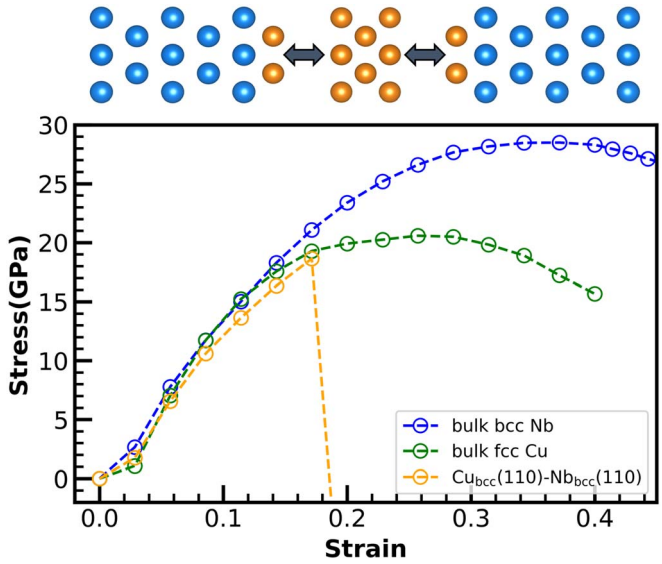

Figure 5. Stress-strain curves calculated by uniaxial simulation for bulk bcc Nb, fcc Cu and $Cu_{bcc}(110)$–$Nb_{bcc}(110)$ interface 1.

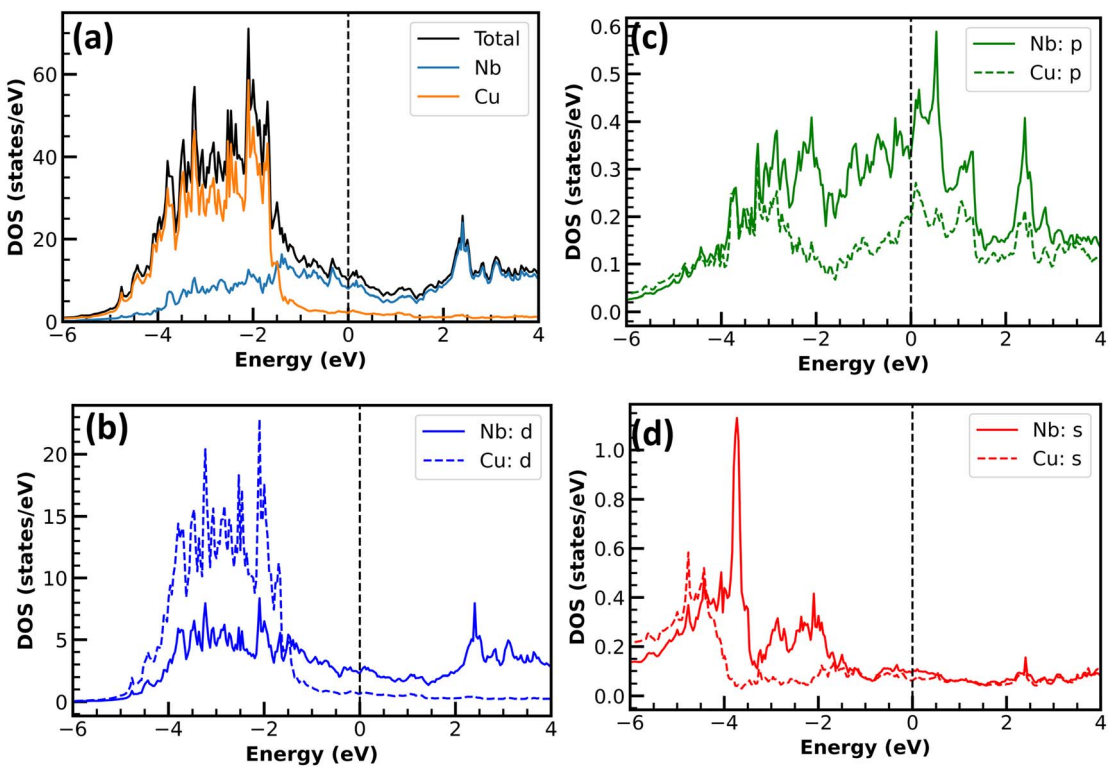

Figure 6. Total and orbital projected electronic density of states for the first neighbouring interfacial Cu and Nb atoms in $Cu_{bcc}(110)$–$Nb_{bcc}(110)$ interface 1 system.

to external deformation and hence its strength is also smaller than stable bulk fcc Cu and bcc Nb. Notably, fracture occurs not at the interfacial layer between Cu and Nb, rather, after first neighbouring interfacial layer of Cu. This suggest that Nb atoms are more tightly bound with each other than Cu. Also, first neighbouring interfacial layer of Cu is attached to the adjacent Nb layer more strongly than with the other Cu layers.

Such interesting findings motivated us to probe the nature of atomic interaction around the interface. To that end, we performed electronic density of states (DOS) and charge density difference analysis of this interface. Figure 6 shows total and orbital projected DOS for the first neighbouring interfacial Cu and Nb atoms. Overlap of the Cu and Nb states as shown in these plots is a clear indication of strong interaction between them.

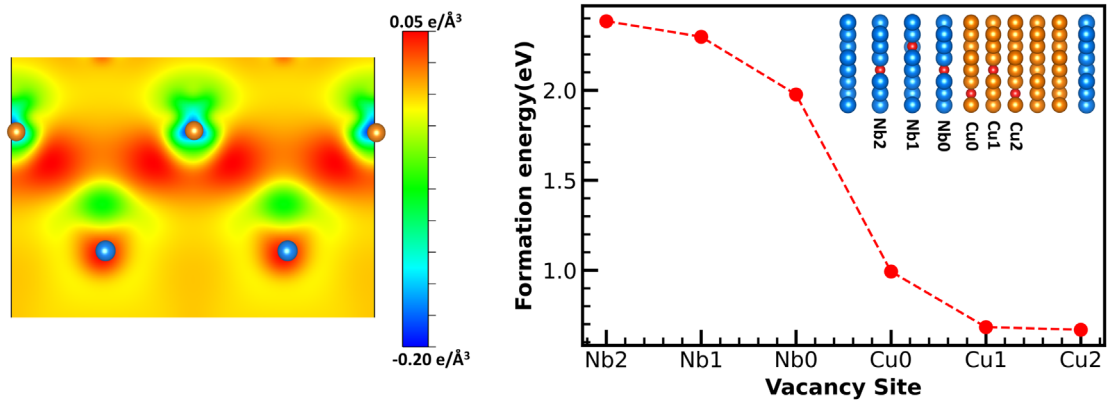

Figure 7. left: charge density difference plot for the Cu_{bcc}(110)–Nb_{bcc}(110) interface 1 showing first neighbouring interfacial Cu and Nb atoms. right: mono-vacancy formation energy at different Cu/Nb layers across the interface. The red dots in the inset images shows the vacancy sites considered in this study.

However, this was not the case for the Nb or Cu atoms sitting away from the interface. This also explains, why fracture occurs after first neighbouring Cu layer. As shown in figure 7 (left) upon formation of the interface charge accumulated regions (red) near the first neighbouring interfacial Cu atoms and charge depleted regions (green) near the Nb atoms has appeared. Based on Bader charge analysis we predicted ~ 0.25|e|/Atom charge transfer from first interfacial Nb atoms to the adjacent Cu atoms.

Finally, we probed defect energetics of Cu–Nb interface 1 by calculating metallic mono-vacancy formation energy at different sites across the interface. As shown in figure 7 (right), formation of a Cu vacancy is more favourable than Nb vacancy. For Cu, vacancy formation energy is same for second and third neighbouring interfacial layers but higher for the first neighbouring interfacial layer. This implies that formation of vacancy at the first neighbouring interfacial layer is no longer the most favourable case as it was reported for the Cu–Nb fcc-bcc interface. Such trend in vacancy formation energy for the Cu layers can be realized from the DOS and charge density difference analysis as discussed above. With this transformed bcc phase of Cu, the Cu atoms at the interface is binding more strongly with the adjacent Nb atoms. Therefore, creating a Cu vacancy by removing one of these Cu atoms sitting at the first neighbouring interfacial layer become more expensive. In case of Cu–Nb fcc-bcc interface, vacancy formation energy was reported lowest for the Cu atoms at the misfit dislocation intersection (MDI) sites at the interface. At the same time energy barrier for a self interstitial to migrate to the interface was also found very low [54]. These two facts together makes a favourable enviournment for both self interstitial and metallic vacancy to meet at the interface and initiate the self annihilation process which is crucial for the material to recover its original strength after high energy neutron irradiation in the proposed fusion reactor enviournment. However, with this transformed bcc Cu phase, as we have shown here, the vacancy formation is no longer most favourable at the interface which will interrupt the self annihilation process and hence degrade the strength of the material.

4. Conclusion

In conclusion, in this study we have investigated the possibility of formation of stable interface between Cu and Nb where one of the component metal is transformed from it's conventional stable phase. Our DFT based strain-energy and DFPT based dynamical stability analysis predicted stable interface between a conventional stable bcc phase of Nb and a transformed bcc phase of Cu. As evidenced by uniaxial tensile simulation this new interface is found weaker than bulk fcc Cu and bcc Nb. However, we observed strong interaction between first neighbouring interfacial Cu and Nb atoms. This along with the calculated vacancy formation energy values confirms change in defect energetics behaviour of this interface compared to fcc-bcc Cu–Nb interface. Such change has a negative impact on self annihilation property of radiation induced defect of Cu–Nb system and hence degrade the strength of the material. These findings clearly indicate that fcc-bcc interface has superior mechanical strength and radiation induced defect resistance property than bcc-bcc Cu–Nb interface. These aspects should be carefully explored in the future design of robust layered material for extreme radiation environment.

Acknowledgments

We would like to acknowledge the computational resources provided by HPC facility Superior at Michigan Technological University, Houghton, MI 49 931-1295, USA and support from Dr S Gowtham from the same University. M B S would also like to acknowledge HPC facility Param-Ishan at Indian Institute of Technology Guwahati, Assam 781 039, India.

Data availability statement

The data cannot be made publicly available upon publication because no suitable repository exists for hosting data in this field of study. The data that support the findings of this study are available upon reasonable request from the authors.

Declaration of competing interest

The authors declare that they have no known competing financial interests or personal relationships that could have appeared to influence the work reported in this paper.

ORCID iDs

Munima B Sahariah https://orcid.org/0000-0002-7392-9940
Ravindra Pandey https://orcid.org/0000-0002-2126-1985

References

[1] Allen T, Busby J, Meyer M and Petti D 2010 Materials challenges for nuclear systems *Mater. Today* **13** 14
[2] Zinkle S J and Busby J T 2009 Structural materials for fission & fusion energy *Mater. Today* **12** 12
[3] Ullmaier H 1984 The influence of helium on the bulk properties of fusion reactor structural materials *Nucl. Fusion* **24** 1039
[4] Knaster J, Moeslang A and Muroga T 2016 Materials research for fusion *Nat. Phys.* **12** 424
[5] Raole P and Deshpande S 2009 Structural materials for fusion reactors *Trans. Indian Inst. Met.* **62** 105
[6] Katoh Y, Snead L L, Henager C H, Nozawa T, Hinoki T, Ivekovi ć A, Novak S and De Vicente S G 2014 Current status and recent research achievements in SiC/SiC composites *J. Nucl. Mater.* **455** 387
[7] Beyerlein I, Caro A, Demkowicz M, Mara N, Misra A and Uberuaga B 2013 Radiation damage tolerant nanomaterials *Mater. Today* **16** 443
[8] Li Z, Cheng J Y, Poplawsky J D, Xu S, Baldwin J K, Beyerlein I J and Mara N A 2023 Critical length scales for chemical heterogeneity at Cu/Nb 3d interfaces by atom probe tomography *Scr. Mater.* **223** 115078
[9] Siegel R, Chang S and Balluffi R 1980 Vacancy loss at grain boundaries in quenched polycrystalline gold *Acta Metall.* **28** 249
[10] Dollar M and Gleiter H 1985 Point defect annihilation at grain boundaries in gold *Scr. Metall.* **19** 481
[11] Mishin Y, Asta M and Li J 2010 Atomistic modeling of interfaces and their impact on microstructure and properties *Acta Mater.* **58** 1117
[12] Hoagland R G and Kurtz R J 2002 The relation between grain-boundary structure and sliding resistance *Philos. Mag.* A **82** 1073
[13] Thyagatur A and Mushongera L T 2023 Effect of interface orientation and loading direction on the mechanical response of Cu–Nb multilayered nanocomposites *J. Mater. Eng. Perform.* **32** 3371
[14] Kaur I, Gust W and Mishin Y 1995 *Fundamentals of Grain and Interphase Boundary Diffusion* (Chichester: Wiley)
[15] Schroeder H, Kesternich W and Ullmaier H 1985 Helium effects on the creep and fatigue resistance of austenitic stainless steels at high temperatures *Nuclear Engineering and Design. Fusion* **2** 65
[16] Mao S, Shu S, Zhou J, Averback R S and Dillon S J 2015 Quantitative comparison of sink efficiency of Cu–Nb, Cu–V and Cu–Ni interfaces for point defects *Acta Mater.* **82** 328
[17] Kang K, Wang J and Beyerlein I 2012 Atomic structure variations of mechanically stable fcc-bcc interfaces *J. Appl. Phys.* **111** 053531
[18] Fu E, Li N, Misra A, Hoagland R, Wang H and Zhang X 2008 Mechanical properties of sputtered Cu/V and Al/Nb multilayer films *Materials Science and Engineering:* A **493** 283
[19] Bodlos R, Fotopoulos V, Spitaler J, Shluger A and Romaner L 2022 Energies and structures of Cu/Nb and Cu/W interfaces from density functional theory and semi-empirical calculations *Materialia* **21** 101362
[20] González C and Iglesias R 2016 Energetic analysis of he and monovacancies in Cu/W metallic interfaces *Mater. Des.* **91** 171
[21] Demkowicz M J and Beyerlein I J 2020 The effects of nanoscale confinement on the behavior of metal laminates *Scr. Mater.* **187** 130
[22] Misra A and Hoagland R 2005 Effects of elevated temperature annealing on the structure and hardness of Copper/Niobium nanolayered films *J. Mater. Res.* **20** 2046
[23] Misra A, Hoagland R and Kung H 2004 Thermal stability of self-supported nanolayered Cu/Nb films *Philos. Mag.* **84** 1021
[24] Ding C, Xu J, Shan D, Guo B and Langdon T G 2021 Sustainable fabrication of Cu/Nb composites with continuous laminated structure to achieve ultrahigh strength and excellent electrical conductivity *Composites Part B: Engineering* **211** 108662
[25] Demkowicz M, Hoagland R and Hirth J 2008 Interface structure and radiation damage resistance in Cu–Nb multilayer nanocomposites *Phys. Rev. Lett.* **100** 136102
[26] Liu X-Y, Uberuaga B P, Demkowicz M J, Germann T C, Misra A and Nastasi M 2012 Mechanism for recombination of radiation-induced point defects at interphase boundaries *Phys. Rev.* B **85** 012103

[27] Misra A, Demkowicz M, Zhang X and Hoagland R 2007 The radiation damage tolerance of ultra-high strength nanolayered composites *JOM* **59** 62
[28] Gao R, Jin M, Li Q-J, So K P, Zhang L, Wang X, Fang Q, Sun C, Shao L and Li J 2021 Hybrid diffusive-displacive helium outgassing in Cu/Nb multilayer composites *Scr. Mater.* **194** 113706
[29] Demkowicz M and Hoagland R 2008 Structure of kurdjumov-sachs interfaces in simulations of a Copper-Niobium bilayer *J. Nucl. Mater.* **372** 45
[30] Mitchell T E, Lu Y C, Jr A J G, Nastasi M and Kung H 1997 Structure and mechanical properties of Copper/Niobium multilayers *J. Am. Ceram. Soc.* **80** 1673
[31] Kung H, Lu Y, Griffin A Jr, Nastasi M, Mitchell T and Embury J 1997 Observation of body centered cubic Cu in Cu/Nb nanolayered composites *Appl. Phys. Lett.* **71** 2103
[32] Wang J, Hoagland R G and Misra A 2008 Phase transition and dislocation nucleation in Cu–Nb layered composites during physical vapor deposition *J. Mater. Res.* **23** 1009
[33] Zhang J, Zhang P, Zhang X, Wang R, Liu G, Zhang G and Sun J 2012 Mechanical properties of fcc/fcc Cu/Nb nanostructured multilayers *Materials Science and Engineering:* A **545** 118
[34] Sasaki M, Koyano M, Negishi H and Inoue M 1988 Fcc niobium films grown by halide chemical vapour deposition on ultrasound-vibrating substrates *Thin Solid Films* **158** 123
[35] Egelhoff W Jr and Jacob I 1989 Reflection high-energy electron diffraction (rheed) oscillations at 77 K *Phys. Rev. Lett.* **62** 921
[36] Costa A, e Castro J D, Muniz R, Ferreira M and Mathon J 1997 Exchange coupling between iron layers separated by bcc Copper *Phys. Rev.* B **55** 3724
[37] Randler R, Dietterle M and Kolb D 1999 The initial stages of Cu deposition on Au (100) as studied by *in situ* STM: the epitaxial growth of bcc Cu *Zeitschrift für Physikalische Chemie* **208** 43
[38] Wang S, Wang H, Du K, Zhang W, Sui M and Mao S 2014 Deformation-induced structural transition in body-centred cubic molybdenum *Nat. Commun.* **5** 1
[39] Hohenberg P and Kohn W 1964 Inhomogeneous electron gas *Phys. Rev.* **136** B864
[40] Giannozzi P, De Gironcoli S, Pavone P and Baroni S 1991 *Ab initio* calculation of phonon dispersions in semiconductors *Phys. Rev.* B **43** 7231
[41] Gonze X and Lee C 1997 Dynamical matrices, born effective charges, dielectric permittivity tensors, and interatomic force constants from density-functional perturbation theory *Phys. Rev.* B **55** 10355
[42] Blöchl P E 1994 Projector augmented-wave method *Phys. Rev.* B **50** 17953
[43] Kresse G and Furthmüller J 1996 Efficient iterative schemes for *ab initio* total-energy calculations using a plane-wave basis set *Phys. Rev.* B **54** 11169
[44] Perdew J P and Wang Y 1992 Accurate and simple analytic representation of the electron-gas correlation energy *Phys. Rev.* B **45** 13244
[45] Monkhorst H J and Pack J D 1976 Special points for brillouin-zone integrations *Phys. Rev.* B **13** 5188
[46] Wang S and Ye H 2003 *Ab initio* elastic constants for the lonsdaleite phases of C, Si and Ge *J. Phys. Condens. Matter* **15** 5307
[47] Kraft T, Marcus P, Methfessel M and Scheffler M 1993 Elastic constants of Cu and the instability of its bcc structure *Phys. Rev.* B **48** 5886
[48] Mouhat F and Coudert F-X 2014 Necessary and sufficient elastic stability conditions in various crystal systems *Phys. Rev.* B **90** 224104
[49] Fei R, Li W, Li J and Yang L 2015 Giant piezoelectricity of monolayer group IV monochalcogenides: SnSe, SnS, GeSe, and GeS *Appl. Phys. Lett.* **107** 173104
[50] Chabungbam S and Sen P 2017 Computational design of a robust two-dimensional antiferromagnetic semiconductor *Phys. Rev.* B **96** 045404
[51] Saikia U, Sahariah M B, González C and Pandey R 2018 Vacancy assisted he-interstitial clustering and their elemental interaction at fcc-bcc semicoherent metallic interface *Sci. Rep.* **8** 3844
[52] Pugh S 1954 Xcii. relations between the elastic moduli and the plastic properties of polycrystalline pure metals *The London, Edinburgh, and Dublin Philosophical Magazine and Journal of Science* **45** 823
[53] Mei W, Wen Y, Xing H, Ou P and Sun J 2014 *Ab initio* calculations of mechanical stability of bcc Cu under pressure *Solid State Commun.* **184** 25
[54] González C, Iglesias R and Demkowicz M 2015 Point defect stability in a semicoherent metallic interface *Phys. Rev.* B **91** 064103